Nimesulide derivatives reduced cell proliferation against breast and ovarian cancer: synthesis, characterization, biological assessment, and crystal structure.

Laila A. Jaragh-Alhadad*, Mayada S. Ali

Dept. of Chemistry, Kuwait University, P. O. Box 5969, Safat 13060, Kuwait

*Corresponding author: laila.alhadad@ku.edu.kw

Abstract

New nimesulide derivatives (A1-A6) were synthesized and investigated by IR, ^{1}H NMR, ^{13}C NMR, melting point, elemental analysis, mass spectra, and DSC analysis. Agent A3 single crystal was grown and solved in a monoclinic crystal system with Cc. Heat shock protein 27 (HSP27) and tubulin are essential cellular proteins for normal cell division and growth. In addition, these proteins are expressed highly in cancer cells. Breast cancer (SKBR3) and ovarian cancer (SKOV3) cell lines are our models for biological assessment. The data revealed that nimesulide analogs showed high cytotoxicity when treated with SKBR3 cell line ranges from 0.22 µM to 12.0 µM, while SKOV3 cell line from 0.1 µM to 16.0 µM. In-depth, structure-activity relationship applied to nimesulide lead structure highlights the importance of a bulk moiety in position two that reduces cell proliferation in both cell lines.

Keywords: Breast cancer; crystal structure; HSP27; nimesulide derivatives; tubulin.

1. Introduction

HSP27 expression is affected by stress conditions such as chemotherapy drugs (Ferms *et al*., 2006; Jego *et al*., 2013; Jaragh-Alhadad, 2018; Venugopal *et al*., 2019). Over-expression of HSP27 in cancer cells causes an anti-apoptotic mechanism (Arya *et al*., 2007; Garrido *et al*., 2006; Paul *et al*., 2010) and cancer cell survival to lethal levels (Lianos *et al*., 2015; Vidyasagar *et al*., 2012) and metastasis (Pavan *et al*., 2013; Zhao *et al*., 2012). Preventing the function of HSP27 can promote cell apoptosis. Clinically, HSP27 is expressed in tumor cells more than benign cells (Langdon *et al*., 1995) such as breast (Vargas-Roig *et al.,* 1998; Kim *et al.,* 2011) and ovarian cancers (Jaragh-Alhadad, 2018; Jaragh-Alhadad *et al*., 2021; Zhao *et al.,* 2012). Nowadays, studies target HSP27 using OGX agents to reduce the cellular stress in both breasts (Zoubeidi & Gleave, 2012) and the prostate (Lamoureux, 2014; Voll *et al*., 2014) cancers. HSP27 inhibition is an attractive therapeutic approach for future treatment because of its association with cell proliferation and survival (Jaragh-Alhadad 2018; Jaragh-Alhadad *et al*., 2021; Kaigorodova *et al*., 2014; Kim. *et al.,* 2011).

Tubulin is a molecular target in cancer because it is associated with cell signaling, mitosis, movement, trafficking, and architecture (Parker *et al.,* 2014; Philippa & Daniel, 2013; Jaragh-Alhadad *et al*., 2021). Clinically, the docetaxel drug is used for breast cancer treatment (Lyseng-

Williamson *et al*., 2005) either in a single treatment or incorporated with other agents. But some patients face drug resistance after the initial treatments (Philippa & Daniel, 2013). Classical tubulin inhibitors cause cell cycle instability and then induce apoptosis (Li & Sham, 2002; Jaragh-Alhadad *et al*., 2021) especially, in solid tumors (Parker *et al.,* 2014). Overexpression of tubulin in ovarian cancer patients causes poor survival rates, so the synthesis of new agents is urgently required (Jaragh-Alhadad *et al*., 2021; Roque *et al*., 2014). This highlights tubulin as a novel therapeutic target for cancer treatments (Giannakakou *et al*., 2000; Jackson *et al*., 2007; Kanthou & Tozer 2009 ; Parker *et al.,* 2014).

It is a perfect strategy to treat breast and ovarian cancer cells with nimesulide derivatives to target multi-cellular proteins in one shot (Jaragh-Alhadad 2018; Jaragh-Alhadad *et al*., 2021). Previously in our project, agents were synthesized to target the functions of two proteins HSP27 and tubulin, and the results were potent and showed cancer cell growth inhibition (Jaragh-Alhadad *et al*., 2021). The new derivatives in the present study examined SKBR3 and SKOV3 as surrogate models, and the results were promising.

2. Experimental

2.1 Material and methods

All chemical analyses were tested and analyzed; at Kuwait University Research Sector Project Unit - RSPU. ^1H and ^{13}C nuclear magnetic resonance spectra possessed using NMR spectrophotometer Bruker, DPX 600 at 600 MHz and 150 MHz in DMSO and $CDCL_3$. Mass spectra; had been received by the GC- MS DFS-Thermo spectrometer, while IR spectra from a Jasco 6300 FT-IR. The DSC curves were recorded on Netzsch DSC 204F1 Phoenix 240-12-0274-L. The single-crystal X-ray diffraction analysis was solved and refined using the Bruker SHELXTL software package.
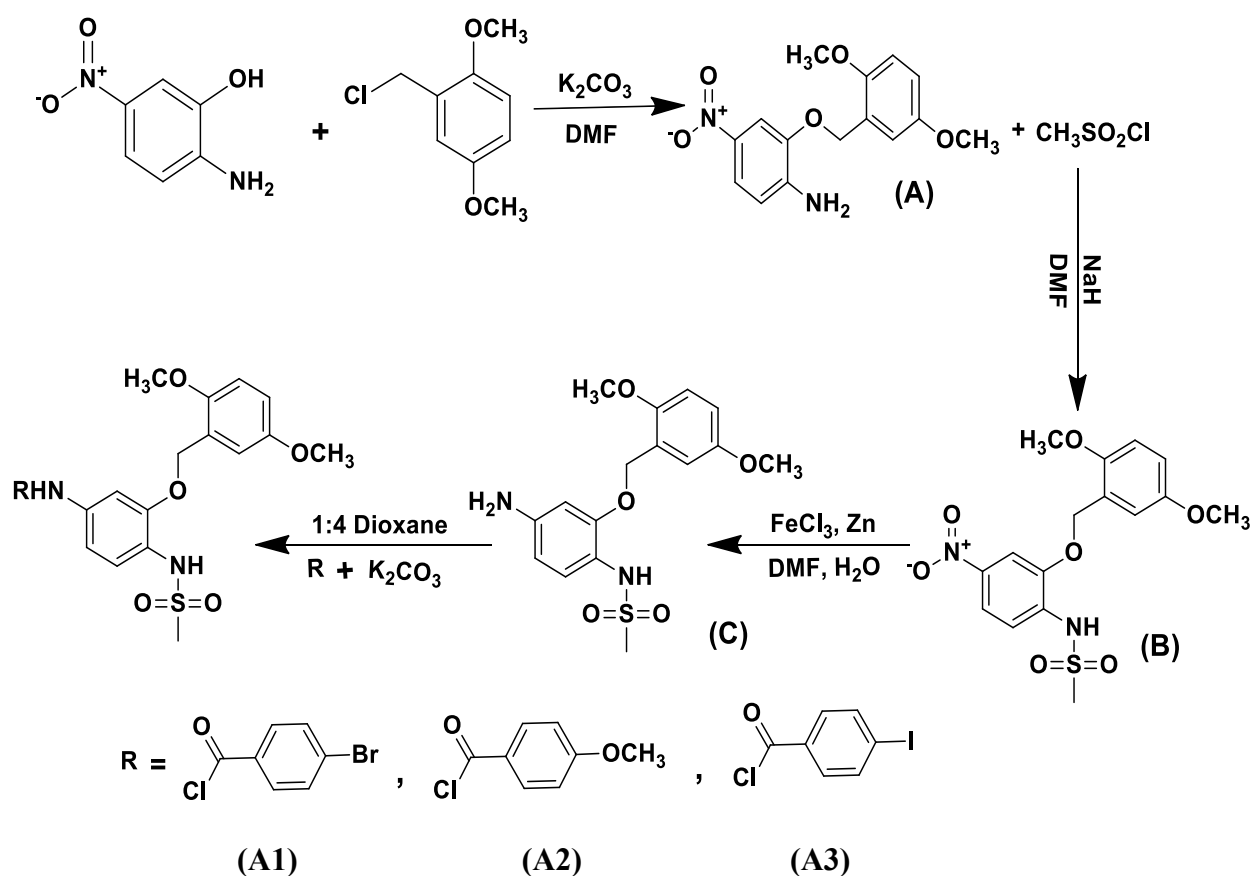
Nimesulide derivatives were designed and synthesized in our laboratory. All chemicals and solvents used for the synthesis were commercially available and were used directly without further preparation.

2.2 Single-crystal data collection and structure refinement

The crystal structure of A3 was grown by dissolving 15.0 mg of it in 1 ml of hot ethanol. Parafilm covered the solution, including holes to allow slow evaporation. A crystal was grown and diffracted within a week by the Bruker SHELXTL Software Package-narrow-frame algorithm. The multi-Scan method (SADABS) determined the data of the absorption. The ratio of minimum/ maximum apparent transmission was equal to 0.571. The calculated minimum and maximum transmission coefficients (based on crystal size) are 0.1970 and 0.5840.

2.3 Synthesis of N-(4-amino-2-((2,5-dimethoxybenzyl)oxy)phenyl)methane-sulfonamide and its derivatives.
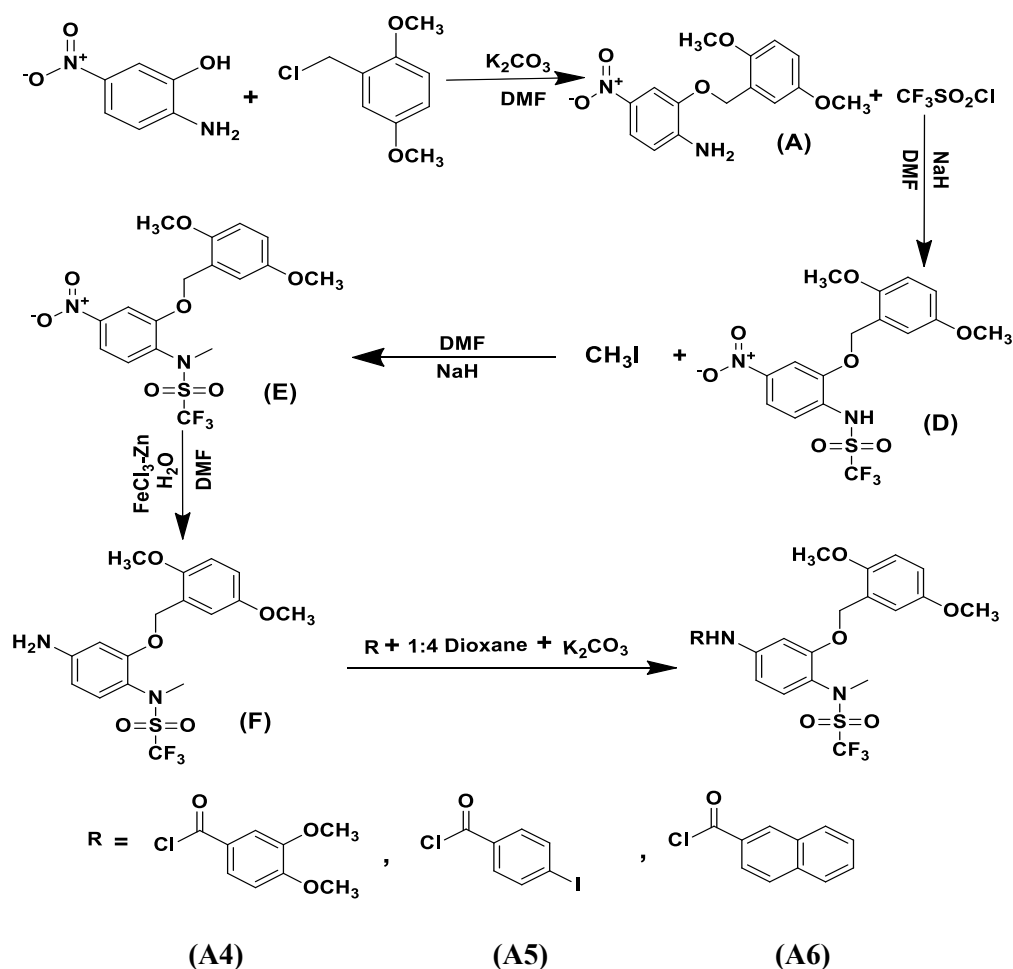
2-Amino-5-nitrophenol (0.154 g; 1 mmol) used as our starting material in (Scheme 1), mixed with 2-(chloromethyl)-1,4-dimethoxybenzene (0.186 g; 1 mmol) with K_2CO_3 (0.138 g; 1 mmol) and DMF overnight. In the next step, both sodium hydride (0.12 g; 5 mmol) and methane sulfonyl chloride (0.114 g; 1 mmol) was added to compound (A) in dry DMF at room temperature to obtain compound (B) within an hour. Then, $FeCl_3$ was added (0.648 g; 4 mmol) with DMF and water and kept stirring for 15 minutes. Then, adding Zn (6.5 g; 10 mmol) to the solution to reduce the nitro group to an amine group to obtain compound (C). Then, different moieties such as 4-bromobenzoyl chloride, 4-iodobenzoyl chloride, and 4-methoxybenzoyl chloride were added to compound (C) (1 mmol) with K_2CO_3 and 1:4 dioxane to obtain the final compounds A1-A3. Synthesis steps carried at room temperature, ligands were precipitated, filtered off, and recrystallized from hot ethanol. Specifically, A3 was grown as a single crystal diffracted.

Scheme 1. Synthesis of N-(4-amino-2-((2, 5-dimethoxy benzyl)oxy)phenyl)methane sulfonamide and its derivatives.

2.4 Synthesis of N-(4-amino-2-((2,5-dimethoxy benzyl)oxy) phenyl)-1,1,1-trifluoro methane sulfonamide and its derivatives.

Step one in scheme 1 is the same. The second step, methane sulfonyl chloride; is replaced by the compound trifluoromethane sulfonyl chloride until we get compound (D), followed by a methylation step with methyl iodide (0.141 g; 1 mmol), sodium hydride (0.12 g; 5 mmol), and DMF to produce compound (E). Then, reducing the nitro group to the amine group to obtain compound (F). Different moieties such as 2-naphthoyl chloride, 3,4-dimethoxybenzoyl chloride, and 4-iodobenzoyl chloride added with (1 mmol), K_2CO_3, 1:4 dioxane were substituted on compound (F) (1 mmol) to obtain the final agents A4-A6 (Scheme 2).

Scheme 2. Synthesis of N-(4-amino-2-((2,5-dimethoxy benzyl) oxy) phenyl)-1,1,1-trifluoro-N-methylmethanesulfonamide and its derivatives.

2.5 Biological studies: cell culture and cell viability

Breast cancer cell line SKBR3 and ovarian cancer cell line SKOV3 were Breast cancer (SKBR3) and ovarian cancer (SKOV3) cell lines from ATCC (Rockville, MD). RPMI1640 medium

supplemented with 10% fetal bovine serum (FBS), used to maintain the cells, two mmol/L L-glutamine; 1 mmol/L sodium pyruvate, 100 U/mL penicillin-streptomycin. FBS heated to inactivate it for 30 min in a 56 °C water bath before use. Cell cultures were grown 5% CO_2 incubator (Bridgeport N.J.). MTT assay was applied using 3-(4,5-dimethylthiazol-2-yl)-2,5-diphenyl-2H- tetrazolium bromide assay in six replicates.

Cells were grown in RPMI1640 medium in 96-well, flat-bottomed plates for 24 h; and were exposed to various concentrations of the agents dissolved in DMSO (final concentration ≤0.1%) in media for 48 hr. The medium was removed, replaced by 200 μL of 0.5 mg/ml of 3-(4,5-dimethylthiazol-2-yl)-2,5-diphenyl-2H-tetrazolium bromide in new media followed by incubation for two hrs. Supernatants; were removed, followed by DMSO addition 200 μL/well. The plate reader; was used to determine the absorbance at 570 nm. Statistical and graphical information was determined using GraphPad Prism software (GraphPad Software Incorporated) and Microsoft Excel (Microsoft Corporation). IC_{50} values were determined using nonlinear regression analysis.

3. Results and discussion

In the present study, six nimesulide derivatives were designed, synthesized, and characterized. Table 1 summarizes the agents' chemical formulae, physical properties, elemental analysis, and molecular weight obtained from mass spectra. Anticancer agents were characterized by IR, ^{1}H NMR, ^{13}C NMR, melting point, and DSC analysis. Molecular weight was confirmed using the GC-MS technique. Additionally, agent A3 single crystal was obtained and crystallographically solved as shown in (Structure 1). Furthermore, the biological assessment targeting both HSP27 and tubulin proteins against breast and ovarian cancer cell lines showed promising anticancer activities based on specific essential bulk moieties.
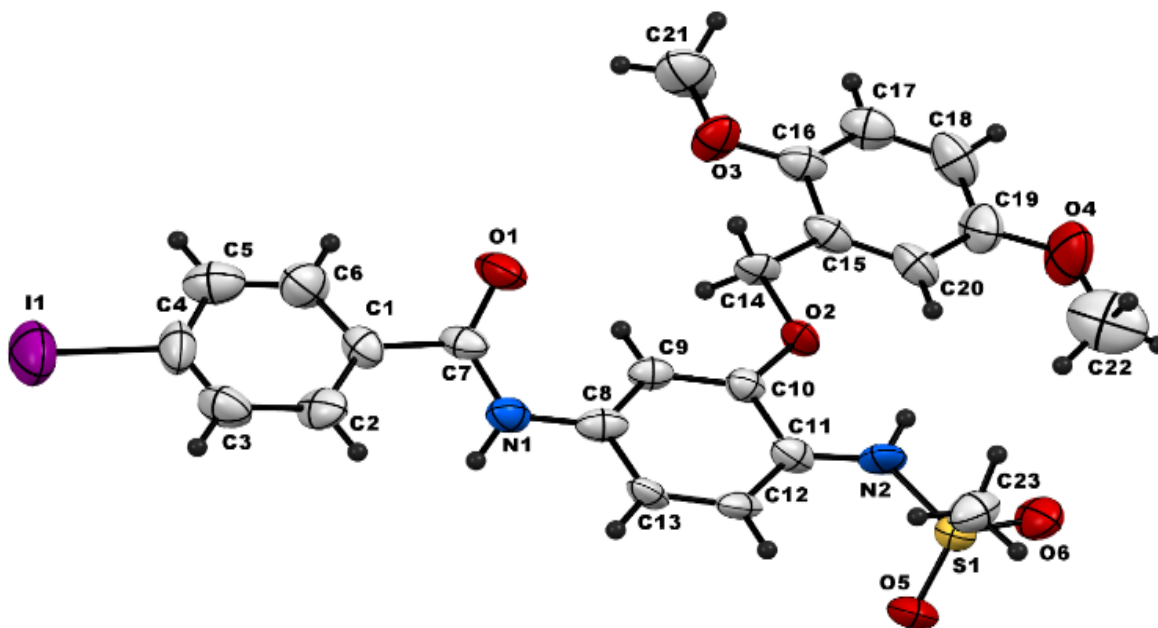
Table 1. Molecular weight and elemental analysis of (A1-A6) agents.

Compound, Empirical formula	M.W., m/e Calcd. (Found)	Color	M.P., °C	C% Calcd. (Found)	H% Calcd. (Found)	N% Calcd. (Found)	S% Calcd. (Found)
A1 $C_{23}H_{23}BrN_2O_6S$	535.41 (535.02)	Pale yellow	218-220	51.60 (51.64)	4.33 (4.31)	5.23 (5.25)	5.99 (5.95)
A2 $C_{24}H_{26}N_2O_7S$	486.54 (486.12)	Paige	231-234	59.25 (59.24)	5.39 (5.40)	5.76 (5.75)	6.59 (6.57)
A3 $C_{23}H_{23}IN_2O_6S$	582.41 (582.39)	Paige	225-227	47.43 (47.42)	3.98 (3.96)	4.81 (4.80)	5.51 (5.52)
A4 $C_{26}H_{27}F_3N_2O_8S$	584.56 (585.09)	Pale yellow	151-153	53.42 (53.40)	4.66 (4.64)	4.79 (4.78)	5.49 (5.47)
A5 $C_{24}H_{22}F_3IN_2O_6S$	650.41 (651.03)	Paige	175-177	44.32 (44.34)	3.41 (3.42)	4.31 (4.33)	4.93 (4.92)
A6 $C_{28}H_{25}F_3N_2O_6S$	574.57 (575.16)	Pale yellow	187-188	58.53 (58.49)	5.39 (5.36)	4.88 (4.84)	5.58 (5.53)

3.1 Crystal structure of N-(3-((2,5-dimethoxy benzyl) oxy)-4-(methylsulfonamido) phenyl)-4-iodobenzamide (A3).

The asymmetric unit of A3 contains two molecules having the same chemical structure but different conformations. One conformer shows all aromatic fragments lying almost in the same plane. At the same time, in the other conformer, the 4-iodophenyl moiety is oriented perpendicular (80.8°) to the plane of the other two phenyl moieties. The different conformational features of these two structures are demonstrated in (Figure 1) where both conformers are overlaid. The crystal packing showed conformers intercalated together, as shown in supporting information. The crystal packing is stable by efficient H-bonding and non-bonding interactions among adjacent molecules. In addition to p-p interactions among the same types of conformers, there are C-H…p interactions between the iodophenyl moieties of different conformations in the crystal network (Figure 2) (Al-Azmi and Mickey 2020).

N-(3-((2,5-dimethoxybenzyl)oxy)-4-(methylsulfonamido)phenyl)-4-iodobenzamide, (A3) is a clear colorless block with the formula $C_{23}H_{23}IN_2O_6S$ and has a molecular weight of 582.39 (Structure 1). It belongs to a monoclinic system with C 1 c 1 space group, as shown in (Table 2). The estimated cell parameters are: a = 54.42(2) Å, b = 4.98(3) Å, c = 18.02(10) Å, α= 90°, ß = 108.17(3)°, γ = 90°. The O4-C16 bond length (1.19 Å) is typical of a delocalized π electron system (1.20 Å). The bond length of S2-O11 and S2-O12 are (1.413; 1.435 Å), which are within the values of the double bond. The bond length of N1-C15 and N2-C12 are almost equal (1.41 and 1.40 Å), while the bond length of I1-C20 is 2.03 Å (Table 3).

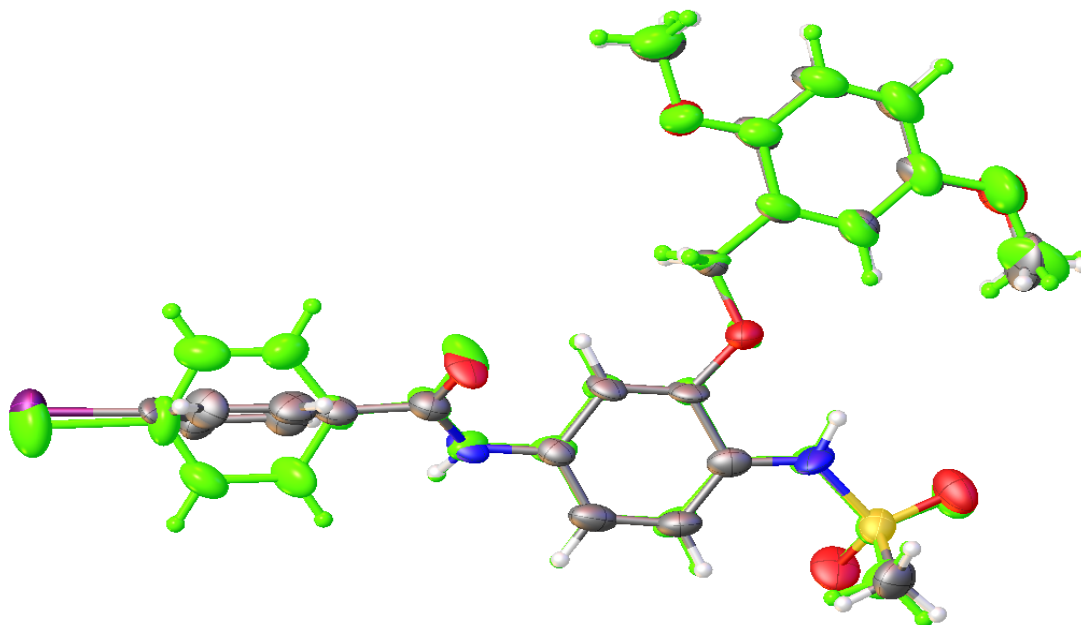**Structure 1.** X-ray crystal structure of agent A3.

Fig. 1. Crystal structure of A3 molecule showing both conformers overlaid to each other. The green-colored conformer has all phenyl groups lying in the same plane, and the multicolored conformer is the structure with 4-iodophenyl fragment oriented almost perpendicular to the plane of the other two phenyl moieties.
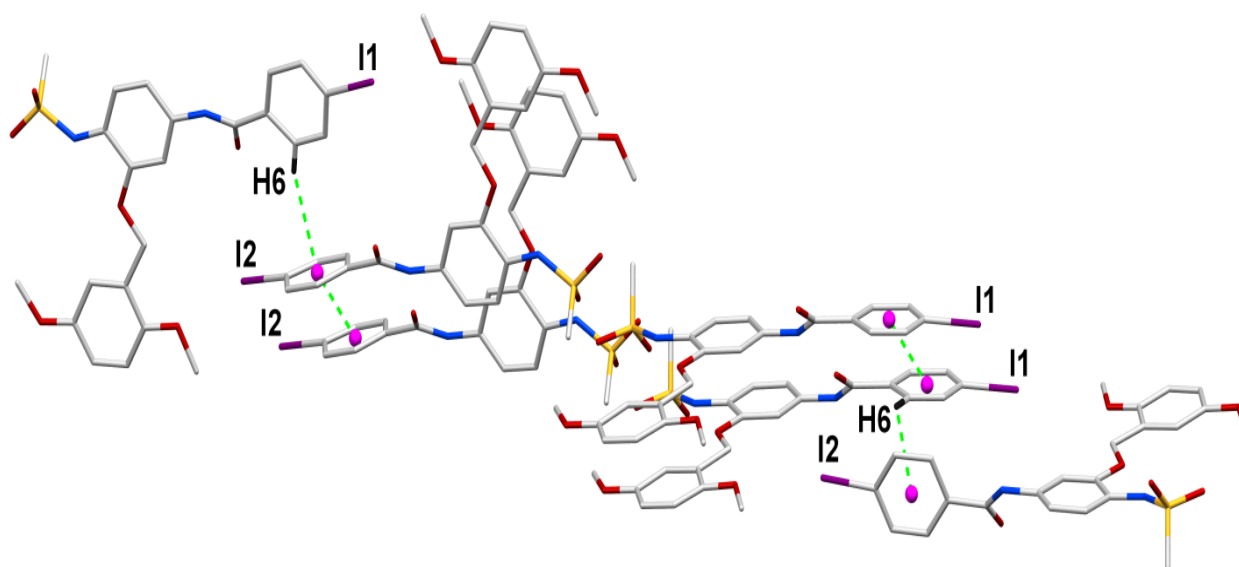

Fig. 2. The Crystal network of A3 molecules showed p-p interactions between 4-iodophenyl moieties of similar conformers and C-H…p interactions between the iodophenyl moieties of different conformers.

Table 2. Data collection and refinement for A3.

Identification code	A3
Empirical formula	$C_{23}H_{23}IN_2O_6S$
Formula weight	582.39
Temperature/K	296(2)
Crystal system	monoclinic
Space group	Cc
a/Å	54.418(3)
b/Å	4.9805(3)
c/Å	18.0143(11)
α/°	90
β/°	108.145(3)
γ/°	90
Volume/Å^3	4639.6(5)
Z	8
ρ_{calc}g/cm^3	1.668
μ/mm^{-1}	12.057
F(000)	2336.0
Crystal size/mm^3	$0.2 \times 0.15 \times 0.05$
Radiation	CuKα (λ = 1.54178)
2Θ range for data collection/°	9.822 to 130.102
Index ranges	$-63 \leq h \leq 63, 0 \leq k \leq 5, -20 \leq l \leq 20$
Reflections collected	6123
Independent reflections	6123 [R_{int} = ?, R_{sigma} = 0.0936]
Data/restraints/parameters	6123/2/602
Goodness-of-fit on F^2	1.049
Final R indexes [I>=2σ (I)]	$R_1 = 0.0832$, $wR_2 = 0.2273$
Final R indexes [all data]	$R_1 = 0.1012$, $wR_2 = 0.2435$
Largest diff. peak/hole / e Å^{-3}	2.22/-0.94
Flack parameter	0.278(7)

Table 3. Bond lengths (Å) and bond angles for A3.

Bond	Length, Å	Bond	Length, Å
S1-O5	1.413(18)	S2-O12	1.435(17)
S1-N1	1.626(14)	O3-C9	1.42(3)
N1-C15	1.41(3)	N2-C12	1.41(3)
O4-C16	1.19(3)	O3-C10	1.41(3)
I1-C20	2.03(2)	S1-C23	1.74(3)
O1-C1	1.24(3)	O2-C4	1.39(4)
Bond	Angle, º	Bond	Angle, º
I1-C20-C21	118.0(15)	C16-N2-C12	123.9(17)
C12-N2-H	118.0	C15-N1-S1	128.2(14)
N1-S1-O6	108.3(9)	N1-S1-O5	107.2(11)
N1-S1-C23	106.8(12)	C10-C3-C9	116.2(14)
C1-O1-C7	115.(2)	C4-O2-C8	121.(3)
C9-O3-C10	116.2(14)	C6-C9-O3	109.3(16)

3.2 Nuclear magnetic resonance (^{1}H NMR and ^{13}C NMR).

The ^{1}H NMR spectra of (A1-A6); were tested in DMSO at 25ºC (Table 4). The spectra of agents A1-A2 (Figures S1 & S2) showed the same signals at 2.86-2.88, 5.09, 3.76-3.73, 7.93-6.88 ppm due to spectrum of CH_3 (sulphonyl), CH_2, OCH_3, and Ar-H while signals at 10.37-10.14 and 9.01-8.97 ppm due to the peak of NH (sulphonyl) and NH (carbonyl) respectively. While the spectra of agents A4-A6 (Figures S3-S5) show signals at 3.36-3.40 ppm due to CH_3 (nitrogen) and only one band for NH (carbonyl) at 10.06, 7.97, and 10.04 ppm. On the other hand, the ^{13}C NMR spectra (Figures S6-S10) showed peaks at 164.49, 153.17, 138.40, 105.21, and 66.33 ppm due to C=O, C-O, C-N, C=C, and CH_3. In the 1H NMR spectra for Ligands (A1-A6), NH (carbonyl) peak showed a signal for one proton, which is a piece of evidence that the reaction occurred and HCl left proved previously in (Jaragh-Alhadad *et al.*, 2021).

Table 4. ^{1}H and ^{13}C NMR signals of the agents.

Agent	NH(S) NH(C)	Ar-H	CH$_2$	OCH$_3$	CH$_3$(S) CH$_3$(N)	^{13}C signals
A1	10.37 (s, 1H) 9.01 (s, 1H)	7.93-6.88 (m,10H)	5.09 (s,2H)	3.76-3.73 (d,6H)	2.88 (s,3H) ---	164.49 (C=O) 153.17 (C-O) 138.40 (C-N) 105.21 (C=C) 66.33 (CH$_3$)
A2	10.14 (s,1H) 8.97 (s,1H)	7.97-6.87 (m,10H)	5.08 (s,2H)	3.84-3.73 (t, 9H)	2.86 (s,3H) ---	164.85 (C=O) 153.17 (C-O) 138.90 (C-N) 105.08 (C=C) 64.87 (CH$_3$)
A4	--- 10.06 (s,1H)	7.80-6.89 (m,9H)	5.13 (s,2H)	3.86-3.73 (m,12H)	--- 3.36 (s,3H)	165.13 (C=O) 154.81 (C-O) 141.74 (C-N) 105.21 (C=C) 65.04 (CH$_3$)
A5	--- 7.97 (s,1H)	7.84-6.84 (m,10H)	5.14 (s,2H)	3.82-3.72 (t,6H)	--- 3.40 (s,3H)	165.23 (C=O) 156.01 (C-O) 140.20 (C-N) 105.69 (C=C) 67.29 (CH$_3$)
A6	--- 10.04 (s,1H)	8.59-6.89 (m,13H)	5.15 (s,2H)	3.80-3.56 (t,6H)	--- 3.36 (d,3H)	165.81 (C=O) 154.87 (C-O) 141.65 (C-N) 105.25 (C=C) 66.33 (CH$_3$)

3.3 Infrared spectra analysis

The major IR bands of agents A1-A6; are listed in (Table 5); their spectrum showed bands at (3276-3382), (1641-1658), (1592-1604), (1216-1232), (755-761), 755 and 748 cm^{-1} attributed to v(NH), v(C=O), v(C-N), v(C-O), v(C-Br) and v(C-I) respectively (Figures S11-S15). The appearance of (SO$_2$) bands at 1382 cm^{-1} due to v_3 asymmetric stretching (1174-1184 cm^{-1}) for v_1, and the v_2 bending region at 507–512 cm^{-1} (Song *et al.*, 2005).

Table 5. IR spectral data (cm^{-1}) of agent A1-A6.

Agent	ν(NH)	ν(C=O)	ν(C-N)	ν(C-O)	ν(SO$_2$)	ν(C-X)
A1	3345br 3276br	1641s	1604m	1216m	1382w,1184w, 512m	755m
A2	3278br	1641s	1604s	1218m	1382m,1182w, 514m	--
A4	3282br	1650m	1596m	1232m	1382m,1184w, 507w	--
A5	3324br	1658s	1592s	1216m	1390s,1180m, 509m	748w
A6	3316br	1654s	1602m	1218w	1390s, 1174m, 507w	--

X= Br, I

3.4 DSC Thermal analysis.

DSC provides the most direct, comprehensive approach for monitoring and interpreting binding interactions involving biological macromolecules. DSC is generally used to measure the partial molar heat capacity over a temperature range of approximately 80 ºC. If a ligand binds to the protein native state, the temperature at which the protein-ligand complex denatures will be higher than the temperature at which the free protein unfolds. DSC thus provides a direct measure of whether ligand binding to a protein is stabilizing or destabilizing. Our agents showed different behaviors in the DSC (Figures S16-S20). The sharp endothermic peaks vary between 150–250°C, and broad exothermic peaks vary between 300–450°C. The first endothermic peak corresponds to the melting of the Agents, while the second peak represents its decomposition.

3.5 Mass spectra analysis of agent A1-A6.

The mass spectrum of agent A1 (Figure S21) showed a molecular peak at m/z = 535.02 (Calcd. 535.41). The other positive ions give peaks at 456 (5%), 184 (20%), 151 (100%), 121 (75%), 91 (15%) mass numbers. The spectrum of agent A2 (Figure S22) showed a signal at m/z = 486.12 (Calcd. 486.54) with 25% abundance. The peaks at 407, 375, 151, 135,121, and 77 are due to the degradation of its species. On the other hand, the MS of agent A4 (Figure S23) represented fragmentation patterns corresponding to the degradation, the first peak at 585.09 (Calcd. 584.56) in agreement with the molecular ion of the agent, and the peaks appeared at 585 (17%), 451, 236 (5%), 151 (100%), 121 (20%) and 69 (10%) mass numbers. The spectrum of agent A5 (Figure S24) displayed multi peaks representing sequential degradation, the molecular peak at m/z = 651 (Calcd. 650.41) with 10% abundance. Also, there are peaks at 230, 151, 121, and 91 mass numbers. Agent A6 MS spectra (Figure S25) showed a peak at 575 with abundance (20%) agreement with calculated molecular weight (574.57), and the other peaks at 441, 151, 121, and 91 represented degradations of the compound. The common ion peak appeared in all spectra at m/e = 151 (calcd 154.12), representing the stable species [$C_6H_6N_2O_3$] with 100% abundance.

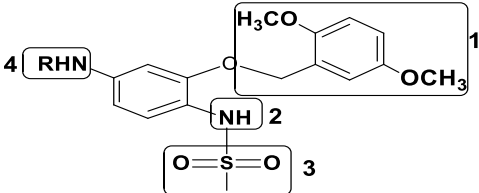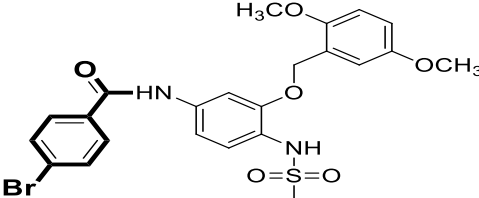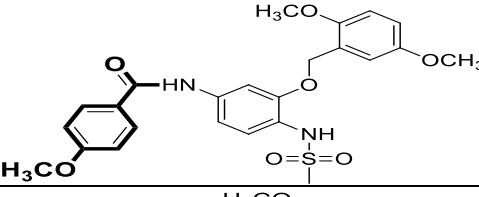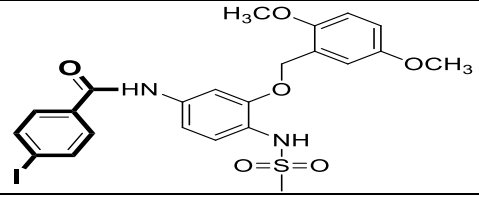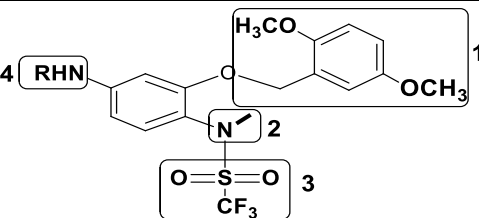3.6 Structure-activity relationship and the biological assessment of the agents
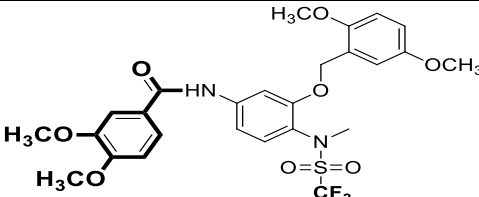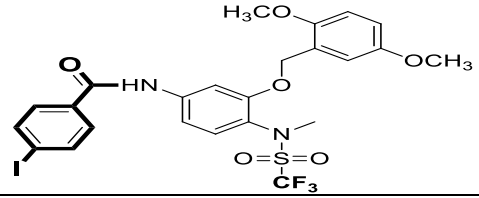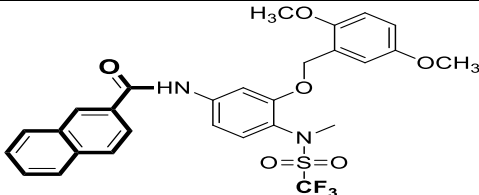
New derivatives of nimesulide targeted both HSP27 and tubulin functions. The new agents in group I and group II inhibited women's cancers cell proliferation at sub-molar levels and showed potent anti-cancer activity (Table 6). In group I, moieties on positions 1, 2 & 3 are fixed, while different moieties are substituted into position 4 (moiety A1: 4-bromophenyl; A2: 4-methoxyphenyl; A3: 4-iodophenyl). The data showed that the IC_{50}s of cell growth inhibition in breast cancer (SKBR3) cell line of agents A1, A2 & A3 ranges from 10.0 μM to 11.0 μM. While, in the ovarian cancer (SKOV3) cell line, agents A1, A2 & A3 range from 5.0 μM to 16.0 μM. These agents showed promising anticancer activity in breast and ovarian cancer due to the essential bulk group in position four.

In group II, moieties on positions 1, 2 & 3 kept the same while different moieties substituted into position 4 (moiety A4: 3,4-dimethoxyphenyl; A5: 4-iodophenyl; A6: 4-napthayl). The data revealed that the IC_{50}s of cell growth inhibition in breast cancer cell line (SKBR3) of agents A4, A5 & A6 range from 0.22 μM to 0.55 μM. While, in ovarian cancer cell-line (SKOV3), agents A4, A5 & A6 range from 0.19 μM to 0.30 μM. Group II moieties' induced apoptosis more than group I. Generally, the data confirmed that -NH moiety reduced the anticancer activity, while the -CH3 moiety increased the anticancer effect in position two. Our synthesized agents showed promising results. Table 6 Biological assessment of SKBR3 and SKOV3 cell lines. IC_{50}: half inhibition concentration- in vitro assessment.

Previously, copper conjugated nimesulide was synthesized and characterized to target the pancreatic cancer cells and the data were promising (Ambike *et al*., 2007). Moreover, nimesulide-loaded nanoparticles were used to treat of prostate cancer and the results showed high cytotoxic activities (Huerta *et al*., 2015). A series of nimesulide derivatives targeted cellular protein HSP27 and HER2 receptor in ovarian cancer cell lines: OVCAR3, HEY1B and SKOV3. The results indicated that down regulation of HSP27 in SKOV3 cells stabilized HER2 receptor expression through HER2 pathway (Jaragh-Alhadad 2018). In 2020, ovarian cancer (SKOV3 cell line) was targeted with nimesulide analogues conjugated to cholesterol loaded into low density lipoproteins as drug delivery strategy and the results were promising (Alhadad *et al*., 2020).

In addition, a research study using nimesulide analogues targeting dual proteins HSP27 and HER2 encapsulated into low density lipoprotein as a vehicle to mimic the native low-density lipoproteins metabolic pathway and the research data were potent (Jaragh-Alhadad 2021). Recently, new modifications were implemented on the nimesulide skeleton to target cellular proteins tubulin and HSP27 in breast (SKBR3) and ovarian (SKOV3) cancer cell lines and the cell's growth inhibition was below two and three μM, respectively (Jaragh-Alhadad *et al*., 2021). Furthermore, those research studies showed how nimesulide and its derivatives are potent anticancer agents.

Table 6. Biological assessment of SKBR3 and SKOV3 cell lines.

		IC$_{50}$ to inhibit SKBR3 cell growth μM	IC$_{50}$ to inhibit SKOV3 cell growth μM
Agent. I		IC$_{50}$ to inhibit SKBR3 cell growth μM	IC$_{50}$ to inhibit SKOV3 cell growth μM
A1		10.2 ± 3.33	16.9 ± 5.2
A2		12.5 ± 6.01 μM	7.75 ± 3.1
A3		11.7 ± 3.33 μM	5.58 ± 0.9
Agent. II		IC$_{50}$ to inhibit SKBR3 cell growth μM	IC$_{50}$ to inhibit SKOV3 cell growth μM
A4		0.44 ± 0.13 μM	0.30 ± 0.09
A5		0.55 ± 0.25 μM	0.19 ± 0.07
A6		0.22 ± 0.09 μM	0.29 ± 0.12

IC$_{50}$: half inhibition concentration- in vitro assessment.

4. Conclusion

Nimesulide drug is known for its antiproliferation activity. Therefore, new nimesulide derivatives were designed, synthesized, characterized, and biologically invitro evaluated on SKBR3 and SKOV3 women cancer cell lines. The structure-activity relationship highlights the importance of position two in groups I and II, which must occupy with -CH_3 for better biological activity. Shortly, new agents with new modifications on nimesulide skeleton were potent targeting female cancers.

ACKNOWLEDGMENTS

Appendix A: Supplementary Material
Single-crystal data for compound N-(3-((2,5-dimethoxy benzyl) oxy)-4-(methylsulfonamido) phenyl)-4-iodobenzamide, is deposited at Cambridge Crystallographic Data Centre (CCDC) under number 2112456. Additionally, NMR, IR, DSC, and mass figures found in supplementary file.

References

Al-Azmi, A., Vinodh, M. (2020). Efficient synthesis of Triazolo[4,5-d] pyrimidine-7-carbonitriles and Imidazole-4,5-dicarbonitriles using Triethylorthoalkylates and their structural characterisation by Single-crystal x-ray diffraction, Kuwait Journal of Science, 48 (2): 1-15. https://doi.org/10.48129/kjs.v48i2.9948.

Alhadad, L. J., Harisa, G. H., Alanazi, F. K. (2020). Design and encapsulation of anticancer dual HSP27 and HER2 inhibitor into low density lipoprotein to target ovarian cancer cells. Saudi Pharmaceutical Journal, 28 (4): 387-396. https//: doi.org/10.1016/j.jsps.2020.01.020.

Ambike, V., Adsulem S., Ahmedmm F., Wang, Z., Afrasiabi, Z., Sinn, E., Sarkar, F., Padhey, S. (2007). Copper conjugates of nimesulide Schiff bases targeting VEGF, COX and Bcl-2 in pancreatic cancer cells. Journal of Inorganic Biochemistry, 101 (10): 1517-1524. https://doi.org/10.1016/j.jinorgbio.2007.06.028.

Arya, R., Mallik, M., Lakhotia, S. C. (2007) Heat shock genes integrating cell survival and death. Journal of Biosciences, 32, 595–610. https://doi.org/10.1007/s12038-007-0059-3.

Ferns, G., Shams, S.,Shafi, S. (2006). Heat shock protein 27: its potential role in vascular disease, Int J Exp Pathol. 87 (4): 253–274. https://doi: 10.1111/j.1365-2613.2006.00484.x.

Garrido, C., Brunet, M., Didelot, C., Zermati, Y., Schmitt, E., Kroemer, G. (2006) Heat Shock Proteins 27 and 70: Anti-Apoptotic Proteins with Tumorigenic Properties, Cell cycle. 5 (22): 2592-2601. https://doi.org/10.4161/cc.5.22.3448.Jackson, J. R., Patrick, D. R., Dar, M. M.,

Huang, P. S. (2007). Targeted anti-mitotic therapies: can we improve on tubulin agents? Nature Reviews Cancer. 7, 107–117. https://doi.org/10.1038/nrc2049.

Huerta, C., Aberturas, M. D. R., Molpeceres, J. (2015). Nimesulide-loaded nanoparticles for the potential coadjuvant treatment of prostate cancer. International Journal of Pharmaceutics, 493 (1-2): 152-160. https://doi.org/10.1016/j.ijpharm.2015.07.027

Jaragh-Alhadad, L. (2018). In-vitro evaluation of HSP27 inhibitors functions through HER2 pathway for ovarian cancer therapy. Transl. Cancer Res., 7 (6): 1510-1517. https://doi: 10.21037/tcr.2018.11.14.

Jaragh-Alhadad, L.; Harisa, G. I.; Alanazi, F. K. (2021). Development of nimesulide analogs as a dual inhibitor targeting tubulin and HSP27 for treatment of female cancers. Journal of Molecular Structure, 1248, 131479. https://doi.org/10.1016/j.molstruc.2021.131479.

Jaragh-Alhadad, L. A. (2021). Encapsulation and in vitro evaluation of low-density lipoprotein with cholesterol conjugated anti HSP27 and HER2 proteins as drug delivery enhancement in ovarian cancer. Biomedical J Sci & Tech Res. 35 (2): 27497-27504. https//:doi.org/ 10.26717/BJSTR.2021.35.005675.

Jego, G.; Hazoumé, A.; Seigneuric, R.; Garrido, C. (2013). Targeting heat shock proteins in cancer. Cancer Letters, 332 (2): 275-285, https://doi.org/10.1016/j.canlet.2010.10.014.

Kaigorodova, E. v.; Bogatyuk, M. V. (2014). Heat Shock Proteins as Prognostic Markers of Cancer. Current Cancer Drug Targets, 14 (8); 713-726. https://doi.org/10.2174/1568009614666140926122846.

Kanthou, C., Tozer, G. M. (2009). Microtubule depolymerizing vascular disrupting agents: novel therapeutic agents for oncology and other pathologies. International Journal of Experimental Pathology, 90 (3): 284-294. https://doi.org/10.1111/j.1365-2613.2009.00651.x.

Kim, L. S.; Kim, J. H. (2011). Heat Shock Protein as Molecular Targets for Breast Cancer Therapeutics. Journal of Breast Cancer, 14 (3): 167-174. DOI: https://doi.org/10.4048/jbc.2011.14.3.167.

Langdon SP, Rabiasz GJ, Hirst GL, King RJ, Hawkins RA, Smyth JF, Miller WR. (1995). Expression of the heat shock protein HSP27 in human ovarian cancer. Clin Cancer Res. 1(12):1603-9. PMID: 9815962.

Lamoureux, F.; Thomas, C.; Yin, M-J.; Fazli, l.; Zoubeidi, A. *et al*. (2014). Suppression of Heat Shock Protein 27 Using OGX-427 Induces Endoplasmic Reticulum Stress and Potentiates Heat Shock Protein 90 Inhibitors to Delay Castrate-resistant Prostate Cancer. European Urology, 66: (1), 145-155. https://doi.org/10.1016/j.eururo.2013.12.019.

Li, Q., and Sham, H. L. (2002). Discovery and development of antimitotic agents that inhibit tubulin polymerization for the treatment of cancer. Expert Opinion on Therapeutic Patents, 12: (11), 1663-1702. https://doi.org/10.1517/13543776.12.11.1663.

Lianos, G. D.; Alexiou, G. A.; Mangano, A.; Mangano, A.; Rausei, s. *et al.* (2015). The role of heat shock proteins in cancer. Cancer letters, 360 (2): 114-118. https://doi.org/10.1016/j.canlet.2015.02.026.

Lyseng-Williamson, K. A., Fenton, C. (2005). Docetaxel: a review of its use in metastatic breast cancer. Drugs, 65 (17): 2513-31. https//:doi: 10.2165/00003495-200565170-00007.
Parker, A. L.; Kavallaris, M.; McCarroll, J. A. (2014). Microtubules and their role in cellular stress in cancer. Front. Oncol., https://doi.org/10.3389/fonc.2014.00153.

Paul, C., Simon, S., Gibert, B., virot, S., Manero, F., Ariigo, A. p. (2010). Dynamic processes that reflect anti-apoptotic strategies set up by HspB1 (Hsp27). Experimental Cell Research, 316 (9): 1535-1552. https://doi.org/10.1016/j.yexcr.2010.03.006.

Pavan, S., Musiani, D., Torchiaro, E., Migliadi, G., Gai, M., Di Cunto, F., Erriquez, J., Olivero, M., Di Renzo, M. F. (2013). HSP27 is required for invasion and metastasis triggered by hepatocyte growth factor. International Journal of cancer, 134 (6): 1289-1299. https://doi.org/10.1002/ijc.28464.

Philippa, C. and Daniel, P. (2013). Tubulin-Targeted Agents Including Docetaxel and Cabazitaxel. The Cancer Journal, 19: (1), 59-. https://doi: 10.1097/PPO.0b013e3182828d38.

Roque, D. M.; Buza, N.; Glasgow, M.; Bellone, S.; Bortolomai, I. *et al.* (2014). Class III β-tubulin overexpression within the tumor microenvironment is a prognostic biomarker for poor overall survival in ovarian cancer patients treated with neoadjuvant carboplatin/paclitaxel. Clin Exp Metastasis, 31: (1): 101–110. https:// doi: 10.1007/s10585-013-9614-5.

Song, Y.; Liu, Z.; Mao, H.; Hemley, R. (2005). High-pressure vibrational spectroscopy of sulfur dioxide. J. Chem. Phys. 122, 174511. https://doi.org/10.1063/1.1883405.

Vargas-Roig, L. M.; Gago, F. E.; Tello, O.; Aznar, J. C.; Ciocca, D. R. (1998). Heat shock protein expression and drug resistance in breast cancer patients treated with induced chemotherapy. Int. J. Cancer (Pred. Oncol.). 79, 468–475 (1998).v https://doi.org/10.1002/(SICI)1097-0215(19981023)79:5<468::AID-IJC4>3.0.CO;2-Z.

Venugopal, A., Sundaramoorthy, K., Vellingiri, B. (2019). Therapeutic potential of Hsp27 in neurological diseases. Egypt J Med Hum Genet 20, 21. https://doi.org/10.1186/s43042-019-0023-4.

Vidyasagar, A.; Wilson, N. A.; and Djamali, A. (2012). Heat shock protein 27 (HSP27): a biomarker of disease and therapeutic target. Fibrogenesis & Tissue Repair, 5 (7): 1-7. https://doi.org/10.1186/1755-1536-5-7.

Voll, E. A., Ogden,I. M., Pavese, J. M., Huang, X., Xu, L., Jovanovic, B. D., Bergan, R. C. (2014). Heat shock protein 27 regulates human prostate cancer cell motility and metastatic progression. Oncotarget, 5 (9): 2648-2663. https: doi: 10.18632/oncotarget.1917.

Zhao, M.; Shen, F.; Yin, Y. X.; Yang, Y. Y.; Xiang D. J. (2012). Increased Expression of Heat Shock Protein 27 Correlates with Peritoneal Metastasis in Epithelial Ovarian Cancer. Reproductive Sciences, 19, 748–753. https://doi.org/10.1177/1933719111432875.

Zoubeidi, A.; Gleave, M. (2012). Small heat shock proteins in cancer therapy and prognosis. The International Journal of Biochemistry & Cell Biology, 44, (10), 1646-1656. https://doi.org/10.1016/j.biocel.2012.04.010.